

ARTICLE OPEN

Assisted reverse electrodialysis—principles, mechanisms, and potential

Marjolein Vanoppen¹, Ella Criel¹, Griet Walpot¹, David A. Vermaas^{2,3} and Arne Verliefde¹

Although seawater reverse osmosis (RO) is nearing its thermodynamic minimum energy limit, it is still an energy-intensive process, requiring 2–3 kWh/m³ at a recovery of 50%. Pre-desalination of the seawater by reverse electrodialysis (RED), using an impaired water source, can further decrease this energy demand by producing energy and reducing the seawater concentration. However, RED is hampered by the initial high resistance of the fresh water source, resulting in a high required membrane area (i.e., high investment costs). In this paper, a new process is presented that can overcome this initial resistance and decrease the RED investment cost without the need for additional infrastructure: assisted RED (ARED). In ARED, a small potential difference is applied in the direction of the natural salinity gradient, increasing the ionic transport rate and rapidly decreasing the initial dilute resistance. This decreasing resistance is shown to outweigh any negative effects caused by, for example, concentration polarization, resulting in a process that is more efficient than theoretically expected. As this effect is mainly important at low dilute concentrations (up to 0.1 M), ARED is proposed as a first step in an economic and energy efficient (A)RED-RO hybrid process.

npj Clean Water (2018)1:9; doi:10.1038/s41545-018-0010-1

INTRODUCTION

Reverse osmosis (RO) is currently the benchmark for seawater desalination, accounting for $\pm 60\%$ of the worldwide desalination capacity.¹ With full-scale plants needing 2–3 kWh/m³ (at 50% recovery)^{2–4} and pilot plants operating at 1.8 kWh/m³, the RO energy demand is approaching the thermodynamic limit of 1.06 kWh/m³ for seawater desalination.^{2,5,6} To decrease the energy demand beyond this limit, focus will shift to pre-treatment and post-treatment options.²

A potential pre-treatment or better “pre-desalination” option for the RO processes is reverse electrodialysis (RED), which has received significant research attention for the production of sustainable energy from salinity gradients.^{7–10} When feeding RED with seawater and an undesirable fresh waste stream (i.e., not suitable for potable water), this process can be applied for pre-desalination. The benefits of an RED-RO hybrid vs. seawater RO are two-fold: (1) energy is produced in RED, while (2) the seawater concentration is decreased, resulting in a lower RO energy demand. The hybrid combination of RO and RED was first mentioned by Li et al.¹¹ and has been discussed in literature since.¹² RED has also been compared to other osmotic dilution processes, pressure-retarded osmosis (PRO), forward osmosis (FO), and pressure-assisted osmosis (PAO), as a pre-desalination step before RO.^{13–15} Compared to these, RED-RO has one main advantage, when using impaired water as low salinity feed, there is no/limited water transport, and the transported species are different in RED and RO. This leads to a more credible “multi-barrier concept”, providing more than one barrier (RO) to avoid pollutants ending up in the produced drinking water.

Similar to FO/PRO, RED is faced with low transport rates (i.e., mainly occurring in the first stages of RED desalination, where the low salinity compartment and membrane resistance is high),¹⁶ and

the required membrane surface area to reach a certain desalination degree is high. At ion-exchange membrane prices up to €100, the slow transport currently represents the main bottleneck of RED applications in general.^{7,17–19}

In this manuscript, a new mode of pre-desalination to overcome slow transport rates, termed Assisted RED (ARED), is presented. ARED could be compared to RED in terms of the driving force, in the same way as the recently investigated PAO compares to PRO.^{20–22} By applying an external current in the direction of the diffusional ion transport (i.e., along the spontaneous line of transport following chemical potential gradients), the desalination process is “assisted” and the initial high resistance of the dilute feed could be quickly overcome. This results in a decrease in the required membrane area and a more economically viable process. Although the process itself has been mentioned briefly in literature before,^{12,23} here, the experimentally observed behavior of an ARED system is compared to its expected behavior, and—similar to PAO, where there is a synergistic effect of combining hydraulic and osmotic driving forces²⁰—it will be shown how and why the system performs better than just the combination of electric and electrochemical driving forces.

RESULTS AND DISCUSSION

The CVCs of the stacks for the both membrane types and the theoretical ideal, and expected CVCs (gray) are shown in Fig. 1. All curves intersect the x-axis at the open-circuit voltage and the y-axis at the short-circuited point (i.e., the maximum current density attainable when the electrodes are short-circuited). Every quadrant represents a different mode of stack operation. The first quadrant represents ED (positive current and voltage), the fourth quadrant represents RED (negative current, positive voltage), and

¹Particle and Interfacial Technology Group, Gent University, Ghent, Belgium; ²Chemical Engineering department, Delft University of Technology, Delft, The Netherlands and

³AquaBattery B.V., Lijnbaan 3 C, Leiderdorp, The Netherlands

Correspondence: Marjolein Vanoppen (marjolein.vanoppen@ugent.be)

Received: 21 November 2017 Revised: 31 January 2018 Accepted: 8 February 2018

Published online: 14 June 2018

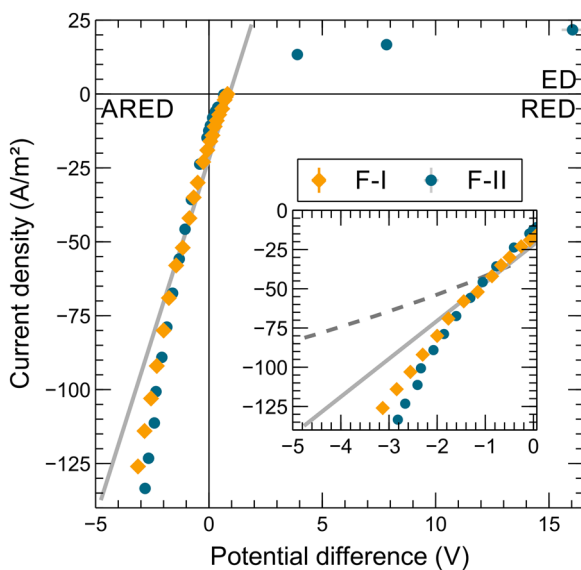


Fig. 1 Current–voltages curves, theory vs. practice. Current–voltage relation using synthetic fresh water and seawater for two different membrane types (diamonds = F- I, circles = F- II), compared to the ideal theoretical curve (gray line). Error bars representing the standard deviation on the potential measurement are obscured by the symbols (the highest error recorded is 0.48 V in the ED region, all other errors are below 0.04 V). The inset shows a close-up of the ARED region (third quadrant), with the dotted line representing the expected effect of concentration polarization. Feed concentrations are 0.5 M NaCl (artificial seawater) and 0.01 M NaCl (artificial impaired water). ED was not performed for F-I type membranes

the third represents ARED (negative current and voltage). Operation in the second quadrant is physically impossible. In ED, the non-ideal behavior becomes clear as the measured points highly deviate from the ideal curve due to strong concentration polarization in the fresh water compartment that is even further desalinated. In RED, losses are expected to be minimal due to the low currents generated.

Whereas in ED the potential difference increases with increasing current densities relative to the ideal curve, the opposite is observed for ARED. Based on Ohm’s law ($U = I \times R$), the resistance of the system in ARED is lower than what would be expected from the theoretically ideal curve, with potentials up to 5.6 times lower. In other words, any (non)-Ohmic losses encountered in the system (e.g., concentration polarization) are counteracted by a stronger, positive effect. This can be explained by two phenomena. First, ions move to the dilute compartment in ARED and RED, increasing the average concentration (between inlet and outlet) in the low salinity compartment. This is most pronounced in ARED as the effect increases with increasing current density. The higher salt concentration increases the electrical conductivity (resulting in a lower Ohmic resistance) of the compartment. Operation in ARED also causes a second effect. Geise et al.¹⁶ showed that membrane resistances measured with a low and high salinity concentration on both sides of the membrane were greater than those with the high concentration on both sides of the membrane. Similarly, Galama et al.²⁴ report that at ionic concentrations below 0.3 M NaCl, the membrane resistance is mainly determined by the lowest external concentration. It can thus be assumed that the increased low salinity compartment concentration in ARED not only results in a lower resistance of the compartment itself, but also of the membranes. Both the effects are counterbalancing and even overwhelming the non-Ohmic losses encountered in the system because the relation between solution concentration and compartment, and membrane resistance is a negative power function, as shown by Galama et al.²⁵ Since ARED rapidly changes

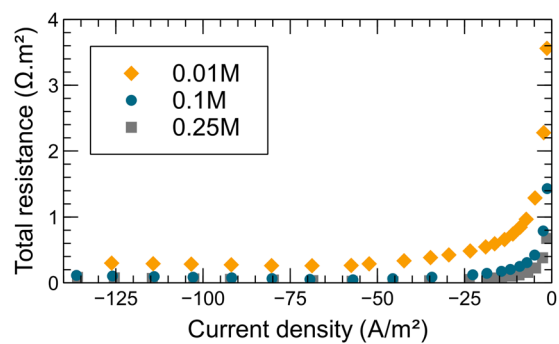


Fig. 2 Total resistance at different current densities. Total resistance (assumed equal to the sum of the low salinity compartment and membrane resistances) for F-I membranes at a fresh water concentration of 0.01, 0.1, and 0.25 M NaCl (flow rate = 100 ml/min)

the low concentrations, resistance rapidly decreases, resulting in better-than-expected performance.

Figure 2 visualizes the total resistance (approximated as the sum of the membrane and low salinity compartment resistance) for different dilute concentrations, based on the continuous experiments. The average membrane resistance can be calculated from the obtained data using Eq. 2. The low salinity resistance is based on the average of the incoming and outgoing concentrations. Three different concentrations are used as the low salinity compartment concentration; 0.01 M (i.e., representing the first stage of (A)RED when feeding with seawater and fresh impaired water), 0.1 and 0.25 M (i.e., further steps in the (A)RED desalination process). As the current density increases (i.e., moving from the RED to the ARED region), the desalination rate in the stack increases, increasing the average dilute concentration. This decreases the solution resistance, resulting in a decrease in membrane resistance, as discussed before. The total resistance decreases via the negative power function and reaches a plateau at higher current densities.

The average membrane resistance provided by the manufacturer is $1 \Omega \cdot m^2$ for the F-I type membranes. From the measurements at low currents (right side of the figure, where the effect of desalination on the resistance is limited), it is shown that a similar resistance was obtained in the 0.25 and 0.1 M solutions, but that the membrane resistance was significantly higher in the 0.01 M solution, as predicted. In the far ARED region (at higher current densities), the overall resistance change is small, while in the RED and initial ARED region (at lower current densities), the membrane resistance significantly decreases with increasing current density. These results further confirm the decrease in resistance of both membrane and solution resistance for higher current densities, especially at low salinities, and thus the reason ARED outperforms its theoretical potential.

If the good performance of ARED is indeed due to the increasing concentration in the dilute and the resulting decrease in resistance, it should level off at higher dilute concentrations. This is confirmed in Fig. 3, where the high salinity concentration was kept constant at 0.5 M to ensure that the effects seen can be attributed to the dilute compartment only.

The CVC profiles shift to lower potential differences with increasing concentration due to a decrease in salinity gradient between the both compartments. This results in a decreased driving force for ion transport, and thus a lower potential difference. This effect causes the slope of the curves to be lower at higher concentrations as well.

More important, the curvature of the curves differs. At the lowest concentrations (0.01 and 0.05 M), the downward trend is clear, both visually and from the second order coefficients (-6.72 to -3.48) of the polynomial fit (equations of polynomial fits are included in Supplementary Table 1). At higher concentrations, the

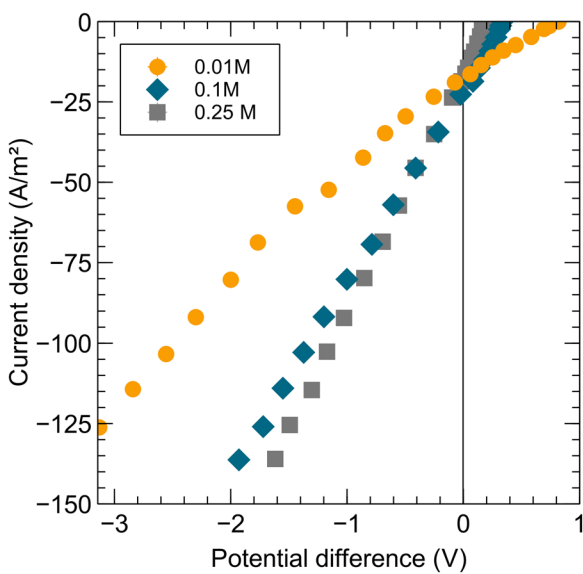


Fig. 3 Comparison of different low salinity concentrations and membrane types. CVCs at different low-salinity compartment concentrations for F-I and F-II type membranes. Error bars representing the standard deviation on the potential measurement are obscured by the symbols (all errors are below 0.04 V)

fit becomes linear because the effect of ion transport on the dilute concentration is less, as the concentration initially was already higher (i.e., solution and membrane resistance are approaching a constant value). The results are similar for both membrane types, although the absolute slope and second order coefficient differ because of the difference in resistance between both membrane types (lower for the F-I membranes).

A key observation is that the increased conductivity of solution and membranes dominates the concentration polarization effects. Concentration polarization would cause a convex curve, while Fig. 3 shows concave curves or close to linear for higher concentrations. In contrast, for ED, it is common to observe higher resistances for higher current densities, which finally leads to a limiting current density.^{26,27} With this knowledge, the ARED conductance can be further increased (i.e., further lowering the cell voltage) by optimizing the intermembrane distance²⁸ and membrane thickness.²⁹

This study shows the potential of ARED, as this system is capable of providing a boost in (pre-) desalination rates in (A)RED-RO hybrids at lower energy (and investment) costs than theoretically expected. Although previous research has theoretically indicated that the thermodynamic energy demand of ARED-RO hybrids is significantly lower compared to stand-alone RO,¹² this research has shown that the benefits of lower than expected resistances in the ARED technique is most pronounced at lower dilute concentrations. At these concentrations, the decrease in solution and membrane resistance significantly reduces the added energy requirement (beyond the theoretical expectations), while at higher concentrations, this benefit is lost and the systems behave as theoretically expected. In our opinion, ARED can thus be best used to overcome the initially high resistance in RED systems. An added advantage is that ARED does not require additional stacks, as segmented electrodes^{30,31} can provide the different potentials to different parts of the stack. In this case, a high potential difference can be applied in the first part of the membrane pile, switching to RED further on in the stack. This can significantly reduce the (A)RED membrane requirement in an RO hybrid, otherwise caused by very low desalination rate in early RED stages. As such, ARED has a defined and valuable niche, as it can help bring (A)RED-RO hybrids closer to the market—although

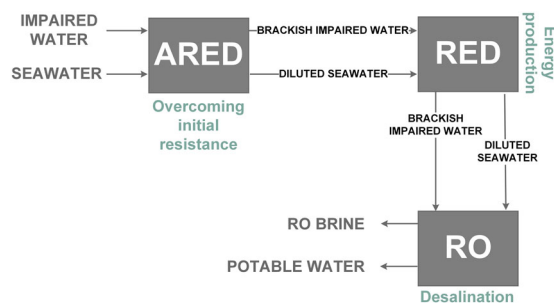


Fig. 4 Envisioned process scheme. Envisioned hybrid process including ARED and RED as pre-desalination steps prior to RO. Impaired water is the preferred fresh water source here, serving as a sink for the ions

Table 1. Nomenclature

Symbol	Description	Unit
A_m	Active membrane area	m ²
C	Concentration	mol/l
E_{ocv}	Open circuit voltage	V
F	Faraday constant	96 485 C/mol
H	Compartment thickness	m
N	Number of cell pairs	–
R_{AEM}	AEM resistance	Ω m ²
R_{CEM}	CEM resistance	Ω m ²
R_g	Universal gas constant	8.314 J/(mol K)
R_{stack}	Stack resistance	Ω m ²
T	Temperature	K
z	Ion valence	–
α	Permselectivity	–
β	Shadow factor	–
ϵ	Spacer porosity	–
κ	Conductivity	S/m

there also could be some potential in ARED-RED sequences, even for sustainable energy production.³² We expect (A)RED-RO hybrids to provide energy-efficient and more economical seawater desalination systems (Fig. 4) that can provide sustainable solutions for water scarce regions worldwide.

METHODS

All symbols and parameters used are reported in Table 1.

Experimental set-up

The electrochemical membrane cell used in the experiments consisted of a plexiglass encasement, containing stretched titanium electrodes with an iridium (anode) or ruthenium (cathode) MMO coating (Magneto Special Anodes B.V., The Netherlands). Five cell pairs, formed with Fujifilm type I (F-I) or type II (F-II) membranes (Fujifilm, the Netherlands), with an active surface area of $7.8 \times 11.2 \text{ cm}^2$ for each membrane, were used. Polyamide spacers provided a compartment thickness of 485 μm. The properties of the membranes and the spacers are included in Supplementary Tables 2 and 3.

To isolate the losses associated to redox reactions occurring at the electrodes, a reference electrode (Ag/AgCl, RE-5B, BASi, USA) was inserted in both end plates to measure the actual potential difference across the cell pairs. The potential difference was recorded using an Agilent 34970 A Data Acquisition/Data Logger Switch Unit (Agilent Technologies, USA). The limit of this equipment ($\pm 1.2 \text{ A}$ or $\pm 136 \text{ A/m}^2$) was used as the endpoint in

the continuous experiments—see further. A DC current was applied to the stack using an adjustable DC power supply (PS 5005, HQ Power, Belgium).

Experimental conditions

Continuous experiments (i.e., the concentration of the feed entering the stack remained constant throughout the experiments) were performed to generate current-voltage curves (CVC), whereby the response of the potential to a change in current was recorded. Synthetic seawater (0.5 M NaCl) and synthetic fresh water (different NaCl concentrations) were used as feed streams. All streams had a flow rate of 100 ml/min and were run through the stack without recirculation. Only the electrolyte solution (0.25 M NaCl) was recycled in the same container. The current was adjusted stepwise, and the corresponding potential was recorded after stabilization of the signal (i.e., a standard deviation <5% between five consecutive measurements, collected every 30 s). The conductivity of NaCl solutions at the inlet and outlet were measured using a conductivity probe (SK23T, Consort, Belgium).

CVCs allow the assessment of the behavior of the ARED technology and comparison to RED and ED. An ideal CVC, assuming a perfect system without losses, is a straight curve, as based on Eqs. 1–3. Deviations from this curve can be caused by changes in the stack resistance, R_{stack} (e.g., because of concentration polarization), and as such provide information on the efficiency and losses encountered in real systems.

$$E_{\text{stack}} = E_{\text{OCV}} + i \times R_{\text{stack}} \quad (1)$$

Here, i (A/m^2) is the current density, while E_{OCV} and R_{stack} are defined by the following equations.³³

$$R_{\text{stack}} = \frac{N}{A_m} \left(\frac{R_{\text{AEM}}}{1 - \beta} + \frac{R_{\text{CEM}}}{1 - \beta} + \left(\frac{h_c}{\kappa_c \times \varepsilon^2} \right) + \left(\frac{h_d}{\kappa_d \times \varepsilon^2} \right) \right) \quad (2)$$

$$E_{\text{OCV}} = N \times a \frac{R_g T}{zF} \ln \left(\frac{C_c}{C_d} \right) \quad (3)$$

N (-) is the number of cell pairs, A_m (m^2) is the active membrane surface area for one membrane, R_{AEM} and R_{CEM} ($\Omega \text{ m}^2$) are the membrane resistances for the anion-exchange membranes (AEM) and cation-exchange membranes (CEM), β (-) is the spacer shadow factor, h (m) is the compartment thickness, subscript C denotes the concentrate compartment and subscript D denotes the dilute compartment, κ (S/m) is the conductivity of the solutions, and ε (-) is the spacer porosity. a (-) is the permselectivity, R_g (8.314 J/(mol.K)) is the universal gas constant, T (K) is the temperature, z (-) is the ion valence, F (96,485 C/mol) is the Faraday constant, and C (mol/m^3) is the concentration.

Data processing and visualization. All data was processed using Microsoft Excel (2016). Where mentioned, polynomial fits were determined using the trendline function. All graphs were constructed using Veusz (version 1.26.1).

Data availability statement

Any raw data used in this manuscript can be freely obtained by contacting the corresponding author.

ACKNOWLEDGEMENTS

Fujifilm is thanked for providing the membranes used in this study. Leo Gutierrez is warmly thanked for his initial review of the paper. This work was funded by the EFRO Interreg V Flanders-Netherlands program under the IMPROVED project.

AUTHOR CONTRIBUTIONS

M.V. was responsible for the writing of the manuscript and guided the experimental research, which was executed by E.C. and G.W. Significant scientific input was delivered by D.A.V. through careful revision of the manuscript and scientific discussion, and by A.V., as head of the research group, through thorough scientific discussion and revision of the manuscript.

ADDITIONAL INFORMATION

Supplementary information accompanies the paper on the *npj Clean Water* website (<https://doi.org/10.1038/s41545-018-0010-1>).

Competing interests: The authors declare no competing interests.

Publisher's note: Springer Nature remains neutral with regard to jurisdictional claims in published maps and institutional affiliations.

REFERENCES

- Ghaffour, N., Missimer, T. M. & Amy, G. L. Technical review and evaluation of the economics of water desalination: current and future challenges for better water supply sustainability. *Desalination* **309**, 197–207 (2013).
- Elimelech, M. & Phillip, W. The future of seawater desalination: energy, technology, and the environment. *Science* **333**, 712–7 (2011).
- Greenlee, L. F., Lawler, D. F., Freeman, B. D., Marrot, B. & Moulin, P. Reverse osmosis desalination: water sources, technology, and today's challenges. *Water Res.* **43**, 2317–48 (2009).
- Kalogirou, S. A. Seawater desalination using renewable energy sources. *Prog. Energy Combust. Sci.* **31**, 242–281 (2005).
- Schiermeier, Q. Water: purification with a pinch of salt. *Nature* **452**, 260–261 (2008).
- Semiat, R. Energy issues in desalination processes. *Environ. Sci. Technol.* **42**, 8193–8201 (2008).
- Daniilidis, A., Vermaas, D. A., Herber, R. & Nijmeijer, K. Experimentally obtainable energy from mixing river water, seawater or brines with reverse electrodialysis. *Renew. Energy* **64**, 123–131 (2014).
- Güler, E., van Baak, W., Saakes, M. & Nijmeijer, K. Monovalent-ion-selective membranes for reverse electrodialysis. *J. Memb. Sci.* **455**, 254–270 (2014).
- Hong, J. G. et al. Potential ion exchange membranes and system performance in reverse electrodialysis for power generation: a review. *J. Memb. Sci.* **486**, 71–88 (2015).
- Tedesco, M. et al. Performance of the first reverse electrodialysis pilot plant for power production from saline waters and concentrated brines. *J. Memb. Sci.* **500**, 33–45 (2015).
- Li, W. et al. A novel hybrid process of reverse electrodialysis and reverse osmosis for low energy seawater desalination and brine management. *Appl. Energy* **104**, 592–602 (2013).
- Vanoppen, M. et al. in *Sustainable Energy from Salinity Gradients* (eds Cipollina, A. & Micale, G.) 281–313 (Woodhead Publishing-Elsevier, Mess Business Centre, Royston Road, Duxford, CB22 4QH, 2016).
- Blandin, G., Verlieerde, A. R. D., Tang, C. Y. & Le-Clech, P. Opportunities to reach economic sustainability in forward osmosis-reverse osmosis hybrids for seawater desalination. *Desalination* **363**, 26–36 (2015).
- Sim, V. et al. Strategic co-location in a hybrid process involving desalination and pressure retarded osmosis (PRO). *Membranes* **3**, 98–125 (2013).
- Blandin, G., Verlieerde, A. R. D., Comas, J., Rodriguez-roda, I. & Le-Clech, P. Efficiently combining water reuse and desalination through forward osmosis—reverse osmosis (FO-RO) hybrids: a critical review. *Membranes* **6**, 1–24 (2016).
- Geise, M., Curtis, A. J., Hatzell, M. C., Hickner, M. A. & Logan, B. E. Salt concentration differences alter membrane resistance in reverse electrodialysis stacks. *Environ. Sci. Technol. Lett.* **1**, 36–39 (2014).
- Post, J. W. et al. Salinity-gradient power: evaluation of pressure-retarded osmosis and reverse electrodialysis. *J. Memb. Sci.* **288**, 218–230 (2007).
- Turek, M. & Bandura, B. Renewable energy by reverse electrodialysis. *Desalination* **205**, 67–74 (2007).
- Yun, T., Kim, Y. J., Lee, S., Hong, S. & Kim, G. I. Flux behavior and membrane fouling in pressure-assisted forward osmosis. *Desalin. Water Treat.* **52**, 564–569 (2014).
- Blandin, G., Verlieerde, A. R. D., Tang, C. Y., Childress, A. E. & Le-Clech, P. Validation of assisted forward osmosis (AFO)process: impact of hydraulic pressure. *J. Memb. Sci.* **447**, 1–11 (2013).
- Lutchmiah, K. et al. Continuous and discontinuous pressure assisted osmosis (PAO). *J. Memb. Sci.* **476**, 182–193 (2015).
- Blandin, G., Verlieerde, A. R. D. & Le-Clech, P. Pressure enhanced fouling and adapted anti-fouling strategy in pressure assisted osmosis (PAO). *J. Memb. Sci.* **493**, 557–567 (2015).
- Mei, Y. & Tang, C. Y. Recent developments and future perspectives of reverse electrodialysis technology: a review. *Desalination* **425**, 156–174 (2018).
- Galama, A. H. et al. Membrane resistance: the effect of salinity gradients over a cation exchange membrane. *J. Memb. Sci.* **467**, 279–291 (2014).
- Galama, A. H., Hoog, N. A. & Yntema, D. R. Method for determining ion exchange membrane resistance for electrodialysis systems. *Desalination* **380**, 1–11 (2016).
- Nikonenko, V. V. et al. Desalination at overlimiting currents: state-of-the-art and perspectives. *Desalination* **342**, 85–106 (2014).
- Sistat, P. & Pourcelly, G. Chronopotentiometric response of an ion-exchange membrane in the underlimiting current-range. Transport phenomena within the diffusion layers. *J. Memb. Sci.* **123**, 121–131 (1997).
- Vermaas, Da, Saakes, M. & Nijmeijer, K. Doubled power density from salinity gradients at reduced intermembrane distance. *Environ. Sci. Technol.* **45**, 7089–95 (2011).

29. Güler, E., Elizen, R., Vermaas, D. A., Saakes, M. & Nijmeijer, K. Performance-determining membrane properties in reverse electrodialysis. *J. Memb. Sci.* **446**, 266–276 (2013).
30. Veerman, J., Saakes, M., Metz, S. J. & Harmsen, G. J. Electrical power from sea and river water by reverse electrodialysis: a first step from the laboratory to a real power plant. *Environ. Sci. Technol.* **44**, 9207–12 (2010).
31. Vermaas, D. A. et al. High efficiency in energy generation from salinity gradients with reverse electrodialysis. *ACS Sustain. Chem. Eng.* **1**, 1295–1302 (2013).
32. Weiner, A. M., McGovern, R. K. & Lienhard V, J. H. Increasing the power density and reducing the levelized cost of electricity of a reverse electrodialysis stack through blending. *Desalination* **369**, 140–148 (2015).
33. Vermaas, Da, Guler, E., Saakes, M. & Nijmeijer, K. Theoretical power density from salinity gradients using reverse electrodialysis. *Energy Procedia* **20**, 170–184 (2012).



Open Access This article is licensed under a Creative Commons Attribution 4.0 International License, which permits use, sharing, adaptation, distribution and reproduction in any medium or format, as long as you give appropriate credit to the original author(s) and the source, provide a link to the Creative Commons license, and indicate if changes were made. The images or other third party material in this article are included in the article's Creative Commons license, unless indicated otherwise in a credit line to the material. If material is not included in the article's Creative Commons license and your intended use is not permitted by statutory regulation or exceeds the permitted use, you will need to obtain permission directly from the copyright holder. To view a copy of this license, visit <http://creativecommons.org/licenses/by/4.0/>.

© The Author(s) 2018